

PCCP

Physical Chemistry Chemical Physics

Accepted Manuscript

This article can be cited before page numbers have been issued, to do this please use: S. Ghosh, R. Sharma, S. Adhikari and A. J. C. Varandas, *Phys. Chem. Chem. Phys.*, 2019, DOI: 10.1039/C9CP03171E.



This is an Accepted Manuscript, which has been through the Royal Society of Chemistry peer review process and has been accepted for publication.

Accepted Manuscripts are published online shortly after acceptance, before technical editing, formatting and proof reading. Using this free service, authors can make their results available to the community, in citable form, before we publish the edited article. We will replace this Accepted Manuscript with the edited and formatted Advance Article as soon as it is available.

You can find more information about Accepted Manuscripts in the [Information for Authors](#).

Please note that technical editing may introduce minor changes to the text and/or graphics, which may alter content. The journal's standard [Terms & Conditions](#) and the [Ethical guidelines](#) still apply. In no event shall the Royal Society of Chemistry be held responsible for any errors or omissions in this Accepted Manuscript or any consequences arising from the use of any information it contains.

Journal Name

ARTICLE TYPE

Fully Coupled ($J > 0$) Time-Dependent Wave-Packet Calculations Using Hyperspherical Coordinates for the H+O₂ Reaction on the CHIPR Potential Energy Surface

Sandip Ghosh,^a Rahul Sharma,^b Satrajit Adhikari^{*a} and António J. C. Varandas^{‡c,d}

Quantum dynamics for H+O₂ → O+OH reaction has been extensively studied on the adiabatic ground state of CHIPR [Varandas, *J. Chem. Phys.*, 2013, **138**, 134117] potential energy surfaces by employing coupled 3D time-dependent wavepacket approach in hyperspherical coordinates. Calculations have been performed for all non-zero J values for various initial rotational states of the diatom [O₂($v = 0, j = 1 - 5$)]. State-to-state and total integral cross sections are calculated using fully converged reaction probabilities, where initial state selected and Boltzmann averaged thermal rate constants are also subsequently calculated. Moreover, a comparison of various reaction attributes obtained by using the fully close coupled approach with the ones obtained from the J -shifting approximation and extrapolation scheme is presented alongside other theoretical results and experimental observations.

1 INTRODUCTION

The gas-phase reaction between H(²S) and O₂(³ Σ_g^-) is a crucial one in combustion chemistry. It plays a pivotal role in chain branching during the oxidation of hydrogen as well as in the molecular oxygen consumption during hydrogen-oxygen and methane-oxygen combustion.¹ Thence, it is designated as the “single most important reaction” in the combustion of hydrogen and hydrocarbons. Moreover, the title reaction acts as a prototype for numerous complex forming chemical reactions.² Such important attributes motivated the scientists to study it both experimentally and theoretically. In order to understand the electronic structure of the complex and the energetics of the reaction, there have been several attempts to construct accurate potential energy surfaces (PESs) for the HO₂ system. On the other hand, reactive scattering calculations have been carried out to theoretically understand the experimental kinetic studies of cross sections as well as thermal rate coefficients. Conversely, the reverse reaction plays a vital role in interstellar chemistry, and especially on

the depletion of the terrestrial ozone atmospheric layer.

In order to properly understand the mechanistic pathway of the title reaction, several theoretical calculations have been performed to construct PESs for the HO₂ system with different levels of accuracy. The CHIPR PES is believed to be the most recent and accurate one based on 14070 *ab initio* data points of the XXZLG PES spline grid,³ which were subsequently modelled with the CHIPR method of Varandas.⁴ One of the pioneering electronically adiabatic PESs for HO₂ was reported by Melius and Blint⁵ (MB). Later on, Pastrana *et al.*⁶ reported the DMBE IV surface from accurate *ab initio* data slightly corrected by reproducing limited spectroscopic data, whereas Kendrick and Pack⁷ constructed a diatoms-in-molecules (DIM) type PES, commonly known as DIMKP PES; see also elsewhere⁸ for a multi-sheeted DIM-based DMBE surface. Other *ab initio* surfaces include the TU PES by Troe and Ushakov (TU)⁹ and the XXZLG PES of Xu *et al.*^{3,10} At the same time, a lot of quantum dynamics studies have been carried out on those PESs for the title reaction. To start with, Varandas^{11,12} performed trajectory calculations on the DMBE IV PES and thereafter, utilized an extrapolation method¹¹ to calculate the integral cross sections and temperature dependent rate coefficients from the $J=0$ quantum mechanical reactive probability. On the other hand, a time independent (TI) quantum dynamics study on the same PES had been performed by Pack *et al.*,^{13,14} where they employed the adiabatically adjusting principal-axis hyperspherical coordinates (APH) method. A while later, Duchovic *et al.*¹⁵ carried out quasiclassical trajectory (QCT) calculations for the H+O₂ reaction both on the MB and DMBE IV PESs. In turn, state-to-state re-

^a School of Chemical Sciences, Indian Association for the Cultivation of Science
2A & 2B Raja S. C. Mullick Road, Jadavpur, Kolkata-700032, West Bengal, India

^b Department of Chemistry, St. Xaviers' College, Kolkata-700016, West Bengal, India

^c School of Physics and Physical Engineering, Qufu Normal University, 273165 Qufu, China.

^d Departamento de Química, and Centro de Química, Universidade de Coimbra
3004-535 Coimbra, Portugal

* Corresponding author. e-mail: pcsa@iacs.res.in

‡ Corresponding author. e-mail: varandas@uc.pt

† Electronic Supplementary Information (ESI) available

action probabilities for the title reaction were calculated by Lin *et al.*¹⁶ on the XXZLG PES using TI as well as time-dependent (TD) quantum mechanical methods. Additionally, Bergueno *et al.*¹⁷ extensively investigated the title reaction by using time dependent wave packet (TDWP) and statistical methods to calculate reaction probabilities and integral cross sections. A Lanczos formalism based on Green's function was utilized by Viel *et al.*¹⁸ to perform dynamics calculations on the DMBE IV PES for obtaining $J = 0$ reaction probabilities and thereafter, calculating the thermal rate coefficients by the J -shifting approximation. On the other hand, the effect of initial rotational state excitation on the reactivity of the title reaction has been studied by Guo, Lendvay and coworkers¹⁹ by utilizing statistical phase space theory, the QCT method and the quantum wave packet approach. Furthermore, TI quantum calculations was carried out on the DMBE IV and TU PESs for the computation of $J = 0$ cumulative reaction probabilities and J -shifted rate coefficients. Later on, Lin and coworkers,²⁰ went on to perform both TD and TI quantum scattering calculations on the XXZLG as well as DMBE IV PESs. The effect of initial rovibrational excitation of the reactant O₂ molecule on the state-to-state reaction probabilities as well as J -shifted rate coefficients were duly studied by Quéméner *et al.*²¹ using TI quantum dynamics calculations on the XXZLG and DIMKP PESs, with the results compared to available experimental ones.^{22–24} However, there are only a few calculations for the title reaction with the inclusion of all nonzero J situations. The fully Coriolis coupled TD quantum mechanical methodology was used by Guo and coworkers²⁵ to calculate reaction probabilities for $J \neq 0$ situations. Sun *et al.*²⁶ assigned the relatively short lifetime of the HO₂ intermediate as the origin of nonstatistical nature of the title reaction, which was further supported from the slight forward-backward asymmetry of the calculated differential cross sections. Moreover, total reaction probabilities and cross sections for $J = 0$ and $J > 0$ situations were calculated in a series of studies^{27–29} by Meijer and Goldfield with the aim of investigating the importance of Coriolis-coupling in the title reaction. They have employed TD quantum mechanics with body-fixed (BF) Jacobi coordinates on the DMBE IV PES. Afterwards, by using a TD quantum mechanical method on the DMBE IV, TU and XXZLG PESs, Hankel *et al.*³⁰ were able to calculate reaction probabilities for both $J = 0$ and $J > 0$ cases. Additionally, integral cross sections have been reported by Honvault *et al.*³¹ using reaction probability profiles upto $J = 50$. Calculations on the most recently constructed CHIPR PES have been performed by Teixidor and Varandas,³² who employed the ABC TI quantum scattering code³³ in hyperspherical coordinates. They had evaluated the rate constant profiles by using the J -shifting technique³⁴ and compared those with previous theoretical calculations²¹ on the XXZLG and DIMKP PESs as well as experimental findings.^{35–37} Furthermore, the same authors studied the X+O₂ reaction on CHIPR PES with X being various isotopic variants of H (Mu, H, D and T). Most recently, Adhikari, Varandas and coworkers³⁸ employed the 3D TDWP methodology in hyperspherical coordinates to calculate the $J = 0$ reaction probabilities for the H+O₂ reaction on CHIPR as well DMBE IV PES and evaluated integral cross sections as well as rate coefficients utilizing both the Bowman's J -shifting scheme³⁴ and Varandas'

trajectory-based extrapolation method.¹¹

There are many experimental measurements of thermal rate coefficients and integral cross sections for the title reaction. During mid 1980s, Cohen and Westberg,³⁵ Warnatz³⁷ and later on, Baulch *et al.*³⁶ presented the recommended values of the rate constant for this reaction over the temperature range 250 – 2000 K based on a fit to several experimental measurements starting from 1970s. It is to be noted that experimentally, the temperature dependent rate constant is found to be Arrhenius in nature. Moreover, integral cross sections were measured over a range of collision energies (0.7 – 2.1 eV) by Kessler *et al.*²² On the other hand, Abu Bajeh *et al.*²³ estimated the ICS by using a pulsed laser "pump-and-probe" setup. In turn, Seeger *et al.*²⁴ used a laser photolysis/laser-induced fluorescence (LP/LIF) "pump-probe" technique to measure absolute reaction cross sections for collision energies of 1.0, 1.6 and 1.9 eV.

The literature of quantum mechanical methodologies on triatomic reaction dynamics is quite vast; for a survey, see our previous publications.^{39–41} Suffice it to say that several reactions have been studied by using both 3D and coupled 3D TDWP approaches in Jacobi coordinates.^{42–45} Carrasco and Roncero⁴⁶ proposed the possibility of transforming from reactants to products Jacobi coordinates in order to calculate state-to-state reaction probabilities using a time-dependent method in a body-fixed frame. Lin and Guo⁴⁷ prescribed an efficient wavepacket method based on the Chebyshev propagation scheme to calculate state-to-state differential as well as integral cross sections for atom-diatom collisions. A while later, Sun *et al.*⁴⁸ introduced a reactant-coordinate-based (RCB) wavepacket method to study the atom-diatom reactive system at the state-to-state level using single reactant Jacobi coordinates. On the other hand, Sun *et al.*⁴⁹ applied two variants of the RCB method^{46,48} with Chebyshev real wave packet propagation to calculate various state-resolved attributes. It should be emphasized at this point that the awkward problem of coordinates transformation from the reactants to the products channel is removed by using the coupled Channel (CC) approach in hyperspherical coordinates,^{38–40,50–53} with such formulation becoming most convenient for an equivalent description of all rearrangement channels. Later on, Crawford and Parker⁵⁴ implemented the formalism for adiabatically adjusting the principal axes hyperspherical (APH) coordinate system such as to treat all arrangement channels equivalently and then, calculated state-to-state reaction probabilities for the $J=0$ case. Using the same coordinate system, Zhao *et al.*⁵⁵ performed scattering calculations employing the Chebyshev polynomial expansion and split-operator methods to calculate state-to-state cross sections.

In the CC approach, the computational cost scales as $(J\prod N_i)^3$ with traditional basis functions, whereas with the implementation of FFT algorithm, the cost reduces to $J\prod_i N_i \sum_i \log N_i$ for the grid method, with J being the total angular momentum and N_i the number of basis functions for the i^{th} internal coordinate. The exact solution of 4D quantum mechanical problem of triatomic reactive scattering is formulated in terms of coupled 3D wavepackets, which are represented by the hyperradius (ρ), hyperangles

(θ and ϕ) and K -component waves. Billing and Markovic⁵² were the first to implement such an approach for the simplest cases of $J = 0$ and $J = 1$. Adhikari and Varandas³⁹ took a step further by extending to any $J \neq 0$ situations. The general method so developed has subsequently been applied to the calculation of both adiabatic^{40,50} and non-adiabatic^{41,56} cross section calculations.

In this article, we have extensively studied the following reaction for the formation of OH($^2\Pi$): $H(^2S) + O_2(^3\Sigma_g^-) \rightarrow OH(^2\Pi) + O(^3P)$, by performing coupled 3D TDWP dynamics on the most recent adiabatic CHIPR PES³² of HO₂ with an aim to explore the reaction accurately using fully close coupled (FCC) approach, where a comparison is made with the previous theoretical results obtained by using J -shifting technique³⁴ and the trajectory-based extrapolation method¹¹ as well as other theoretical and experimental findings in the collision energy range 0.0–2.5 eV.

2 THEORETICAL BACKGROUND

The initial wave packet in hyperspherical coordinates can be expressed in terms of 3- j symbol and modified spherical harmonics ($C_{j\mu}$) as follows:

$$\begin{aligned} \Phi_K &= \sqrt{2\pi} \sin \eta J(Rr\eta|\rho\theta\phi)(2l+1)\phi_{vj}(r) \\ &\times \chi(R)(-1)^{j-l} \sum_{\mu} \begin{pmatrix} j & l & J \\ \mu & 0 & -\mu \end{pmatrix} C_{j\mu}(\eta) A_{K\mu}, \end{aligned} \quad (1)$$

where

$$\begin{aligned} A_{K\mu} &= (-1)^K \int_0^{2\pi} d\gamma \int_0^\pi d\beta \sin \beta \\ &\times \exp(-iK\gamma + i\mu\xi) C_{JK}(\beta) C_{J\mu}(\Theta'), \end{aligned} \quad (2)$$

where the geometry of the ABC triangle is monitored by the hyperradius ρ and two hyperangles θ and ϕ , and three external coordinates, namely, the Euler angles α , β and γ defines the orientation of the plane. The orthonormality condition of $A_{K\mu}$ and the initial wavepacket are described elsewhere.^{39,40}

In turn, the Hamiltonian operator of the triatomic system is written in terms of Johnson's hyperspherical coordinates as follows:^{39,57}

$$\begin{aligned} \hat{H} &= -\frac{\hbar^2}{2\mu_R} \frac{\partial^2}{\partial \rho^2} + \frac{2}{\mu_R \rho^2} \hat{L}^2(\theta, \phi) + \frac{\hat{J}_z^2 - \hat{J}_z^2}{\mu_R \rho^2 \cos^2 \theta} \\ &+ \frac{\hat{J}_z^2 - 4 \cos \theta \hat{J}_z \hat{P}_\phi}{2\mu_R \rho^2 \sin^2 \theta} + \frac{\sin \theta}{\mu_R \rho^2 \cos^2 \theta} \frac{1}{2} [\hat{J}_+^2 + \hat{J}_-^2] \\ &+ V_0(\rho, \theta, \phi) + \Delta V(\rho, \theta), \end{aligned} \quad (3)$$

where \hat{J}_+ and \hat{J}_- are the raising and lowering operators, respectively, $V_0(\rho, \theta, \phi)$ is the potential employed in our calculation and all other operators are described elsewhere.³⁹

By substituting the wave packet (Eq. 1) and the Hamiltonian (Eq. 3) into the TD Schrödinger equation (TDSE), the following set of

coupled differential equations is obtained:

$$\begin{aligned} i\hbar \frac{\partial \Phi_K}{\partial t} &= \left\{ -\frac{\hbar^2}{2\mu_R} \frac{\partial^2}{\partial \rho^2} + \frac{2}{\mu_R \rho^2} \hat{L}^2(\theta, \phi) \right. \\ &+ \frac{\hbar K(\hbar K - 4 \cos \theta \hat{P}_\phi)}{2\mu_R \rho^2 \sin^2 \theta} + \frac{\hbar^2 [J(J+1) - K^2]}{\mu_R \rho^2 \cos^2 \theta} \\ &+ V_0(\rho, \theta, \phi) + \Delta V(\rho, \theta) \Big\} \Phi_K \\ &+ \frac{\sin \theta}{\mu_R \rho^2 \cos^2 \theta} [M_{K,K+2} \Phi_{K+2} + M_{K,K-2} \Phi_{K-2}], \end{aligned} \quad (4)$$

where $M_{K,K\pm 2}$ is the coupling term between the K -component waves Φ_K and $\Phi_{K\pm 2}$:

$$M_{K,K\pm 2} = \frac{\hbar^2}{2} \sqrt{(J \mp K)(J \pm K+1)(J \mp K-1)(J \pm K+2)}. \quad (5)$$

By next projecting^{52,58} the time dependent wave packet onto the asymptotic eigenstates at a fixed value of $R (= R^*)$, one obtains time dependent scattering amplitudes for different v', j', l' :

$$\begin{aligned} u_{v'j'l'}^J(R^*; t) &= 4R^* \int dr \int d\eta r \sin \eta \rho^{-5/2} (\sin 2\theta)^{-1/2} \\ &\times \phi_{v'j'}(r) \times \sum_{K\mu} g_{j'l'\mu} A_{K\mu}^*(\eta) \Phi_K(\rho, \theta, \phi), \end{aligned} \quad (6)$$

where the integration is carried out over the (θ, ϕ) grid using the transformation from Jacobi to hyperspherical coordinates.³⁹ The values of Φ_K on the (θ, ϕ) -space at $R = R^*$ are then obtained by interpolating the amplitudes of Φ_K s on the associated space. When the entire wave packet passes through the projection region, the time dependent scattering amplitudes are Fourier transformed from time to energy space:

$$b_{v'j'l'}^J(E; R^*) = \frac{1}{\sqrt{2\pi}} \int dt u_{v'j'l'}^J(R^*; t) \exp(iEt/\hbar). \quad (7)$$

These amplitudes are expanded in terms of incoming and outgoing waves by using spherical Bessel (j_l) and Neumann (n_l) functions:^{39,52,58}

$$b_{v'j'l'}^J = A_{v'j'l'}^{in} k_{v'j'} R h^-(k_{v'j'} R) + A_{v'j'l'}^{out} k_{v'j'} R h^+(k_{v'j'} R), \quad (8)$$

where

$$h^\pm(k_{v'j'} R) = -n_l(k_{v'j'} R) \pm i j_l(k_{v'j'} R), \quad (9)$$

with h^\pm being the Hankel function.

The projection on the incoming component should be zero and therefore, the reaction probability from the initial state (vjl) to the product state ($v'j'l'$), can now be calculated from the ratio of the outgoing and incoming fluxes,

$$P_{v'j'l' \leftarrow vjl} = \frac{F_{v'j'l'}}{F_{vjl}} = \frac{\frac{1}{\mu_{out}} k_{v'j'} |A_{v'j'l'}^{out}|^2}{\frac{1}{\mu_{in}} k_{vj} |c_E^l|^2}, \quad (10)$$

where the scattering amplitude corresponding to the initial wave packet at energy E is c_E^l , and all other terms have their usual meaning. Moreover, the weight in energy space is calculated from

the expression of the weight in k space as:

$$|c_E^l|^2 = \left(\frac{\mu_{in}}{\hbar k} \right)^2 |c_k^l|^2, \quad (11)$$

where $|c_k^l|^2$ is obtained from the analytical expression of a Gaussian wave packet:

$$|c_k^l|^2 = \sqrt{2/\pi} \sigma \exp[-2\sigma^2(k - k_0)^2] \quad (12)$$

Finally, rovibrationally resolved integral cross sections (ICS) can be calculated by summing over the reaction probabilities for all those J values, yielding:

$$\sigma_{v'j' \leftarrow vj}(E_c) = \frac{\pi\hbar^2}{2\mu_R(E - E_{vj})(2j+1)Q_{el}} \sum_{J=0}^{J_{max}} (2J+1) P_{v'j' \leftarrow vj}^J(E_c) \quad (13)$$

where μ_R is the reduced mass for the reactant channel, E_{vj} the energy of the initial state, Q_{el} is 3 in our present case, j'_{max} and v'_{max} are the highest open product rotational and vibrational channels, respectively with highest total angular momentum J_{max} .

In turn, the state-to-state rate constant is obtained by integrating the ICS profiles over the entire collision energy regime:

$$k_{v'j' \leftarrow vj}(T) = \left(\frac{8k_B T}{\pi\mu_R} \right)^{\frac{1}{2}} \frac{1}{(k_B T)^2} \times \int_{E_0}^{E_{max}} dE_c E_c \sigma_{v'j' \leftarrow vj}(E_c) e^{-E_c/k_B T} \quad (14)$$

where E_{max} denotes the highest kinetic energy considered in the calculations, and E_0 corresponds to the threshold collision energy, which is zero for a barrierless reaction.

2.1 Absorbing potential, propagation, projection and computational details

We have used a linear absorbing potential^{59,60} in the hyperradius at each θ and ϕ , thence

$$V_{Im}(\rho) = \begin{cases} V_{opt} \cdot (\rho - \rho_I), & \rho_I \leq \rho \\ 0, & \text{otherwise,} \end{cases}$$

where ρ_I denotes the starting point for such a potential and V_{opt} monitors the minimal reflection of the wave function from the boundary (see Table 1 of the Supplementary Information, SI).

The intrinsically parallel version of the Fast Fourier Transformation (FFT)⁶¹ algorithm is employed to evaluate the kinetic energy operators, where the computational cost scales as $cN \log N$, with N being the total number of grid points on the ρ , θ and ϕ coordinates. The iterative Lanczos reduction technique is utilized for the evolution of the wave packet with time. To minimize the effect of singularities of the Hamiltonian on the wavefunction during the operation of the corresponding kinetic energy operators on the wavefunction using the FFT routine, the range of the hyperangle θ is extended from $\pi/2$ to π and the associated amplitudes on the grid points are taken as the inverse mirror image of those from 0 to $\pi/2$ making the resulting function an odd func-

tion around $\theta = \pi/2$. Such an extension of the domain of θ leads to the sine transformation, where the amplitudes at $\theta = 0, \pi/2$ and π naturally become zero. Moreover, the time propagation of the wave packet by the iterative Lanczos reduction technique is able to monitor the recursion by handling the magnitude of the last few vectors and eventually, keeps very small amplitudes both at $\theta = 0$ and $\pi/2$ due to the utilization of sine transformation technique. Moreover, we have implemented OpenMP-MPI parallelization scheme^{39–41} for further reduction of the computational cost while carrying out the dynamics with inclusion of all helicity quantum numbers as well as multiple electronic states, if involved.

III. Results and discussion

We have performed coupled 3D time dependent wave packet calculations in hyperspherical coordinates for the H+O₂ reaction using the CHIPR PES of HO₂.⁴ Reaction probabilities have been calculated for products formation (O+OH) with non-zero total angular momentum (*i.e.*, $J > 0$) situations by employing the FCC formalism, where using those probabilities, integral cross sections (ICSSs) and temperature dependent rate coefficients are obtained. Indeed, the aim of the present calculation is to investigate the title reaction in the most accurate way (FCC) to explore the validity of previously employed J -shifting approximation³⁴ and Varandas' trajectory-based extrapolation scheme¹¹ in comparison with experimental data. It is noteworthy that only a few attempts were taken for performing reactive scattering calculations including all non-zero total angular momentum cases,^{29,31,62} since an exhaustive quantum dynamics treatment is extremely difficult due to the presence of deep HO₂ potential and heavy mass of O atoms. Our OpenMP-MPI parallelized code comes on rescue since it is really suitable for carrying out scattering calculations at high non-zero J situations. Therefore, in the calculations here reported, we have investigated the title reaction for situations upto $J=45$ involving various initial roto-vibrational states ($v = 0, j=1, 3$ and 5) of the O₂ diatom. All other dynamical parameters employed in our calculations are shown in Table I of the SI.

Total reaction probabilities of the H+O₂ ($v=0, j=1$) reaction for various non-zero total angular momentum cases are shown in comparison with the $J=0$ case³⁸ in Figure 1. When the total angular momentum is increased from $J=0$ to 5, the magnitudes of the reaction probability slightly decrease particularly in the lower energy regime, whereas the $J=10$ profile is almost similar to that of the $J=5$ case. On the other hand, when the J values are further increased upto 15, the reaction probabilities decrease minutely in the moderate collision energy regime (1.2 - 1.8 eV) compared to the $J=10$ case. Moreover, the reaction probabilities for the $J=20$ case decrease further almost in the entire collision energy regime. As expected, the threshold values of the collision energy for the appearance of reaction probabilities gradually shift to larger values, *viz.*, ~ 0.67 eV for $J = 0$ up to ~ 0.8 eV for $J=20$. Indeed, the trends of the profiles from $J=0$ to 15 are more or less consistent with each other, *i.e.* the reaction probabilities gradually increase with the increment of collision energy and finally attain a kind of plateau fluctuating around an average value at the high-

est collision energy regimes. Once again, when the total angular momentum is increased further from $J=20$ to 35, the magnitude of the reaction probabilities generally decrease almost in the entire energy regime. Note that the threshold collision energy also gradually increases with the increment of total angular momentum. It is clearly visible that the total reaction probability profiles diminish further with increasing total angular momentum in going from $J=35$ to 40 and thereafter to 45, indicating the convergence of reaction probabilities with respect to J for the entire collision energy range here considered. It may be noted that although the reaction probability profiles are found to be converged with the basis set $N_p=180$, $N_\theta=64$ and $N_\phi=128$, we perform the dynamics with the larger grid size $256\times 64\times 128$ in order to avoid any possible error due to interpolation of the wavepacket on the $\{\rho, \theta, \phi\}$ -space for the projection on a particular R ($= R^*$).

Figure 2 depicts the total reaction probability profiles for $j = 3$ at various non-zero total angular momentum cases. In this case (unlike for $j = 1$), the reaction probability profile for $J = 5$ is slightly higher from that of $J = 0$, mostly in the lower to moderate collision energy regimes (1.0 - 1.5 eV). On the other hand, in the higher energy regimes, the magnitude of the reaction probability for $J = 5$ is generally lower compared to the $J = 0$ case. As we move towards higher J values upto 20, the magnitudes decrease smoothly over the lower energy regimes, whereas the profiles are fluctuating around an average value (~ 0.55) in the higher energy regimes (1.5 – 2.5 eV). On the other hand, if J is increased further, the threshold value of reaction probability also increases and the probabilities smoothly diminish to a large extent at higher collision energies, indicating the convergence of the profiles. Lastly, Figure 3 shows the total reaction probability profiles for $j = 5$ case with total angular momenta upto 45, where the trends of the profiles are mostly similar to the $j=3$ case. Indeed, as we go towards higher j s, the threshold value of collision energy increases at a higher rate with the increment of J , specifically from 40 to 45, while the resonances in the reaction probability profiles decrease substantially for high J values. It is noteworthy that for $J > 0$, the threshold collision energy increases due to the higher magnitude of the centrifugal barrier. Although the threshold value increases at a slower rate for low $J (< 25)$ values, it grows rapidly for higher J values, *viz.* $J > 25$, due to the quadratic J dependence of the centrifugal barrier.²⁵ Conversely, the magnitudes of the reaction probabilities at moderate to high collision energies (1.7 - 2.5 eV) for higher J s appear to be larger with increasing j states. At this point, it is noteworthy that one needs to consider a lot of higher initial rotational states of O₂ due to the heavy mass of the O atom itself as was investigated elsewhere.^{63,64} However, fully close coupled (FCC) calculations are very difficult to perform while considering higher total angular momentum values. Thus, we have restricted our study by considering the rotational states, namely, 1, 3 and 5 in order to understand the effect of initial rotational excitation of the reactants on the various reaction attributes and, at the same time, find a comparison with the existing theoretical calculations and experimental measurements.

For any quantum dynamics calculations, it is necessary to study the convergence profiles of reaction probabilities. In Figure 4, we

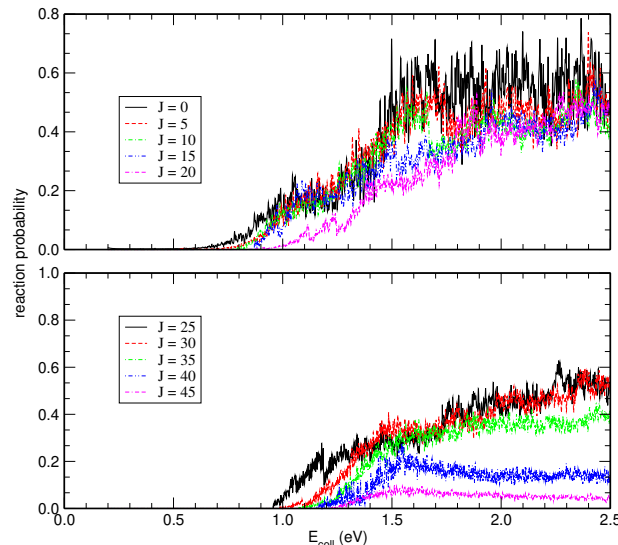
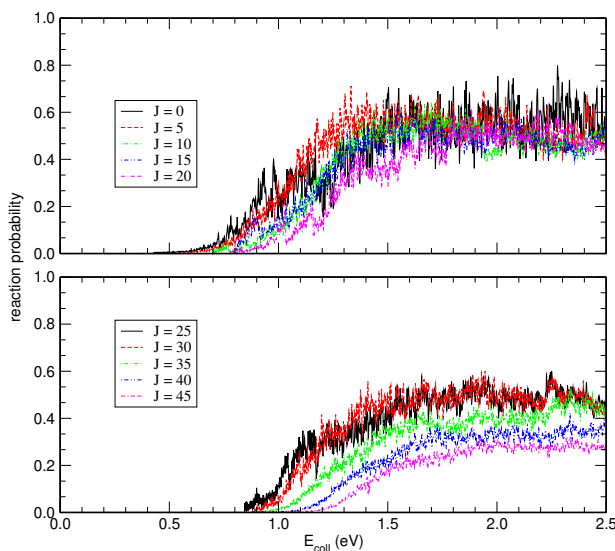
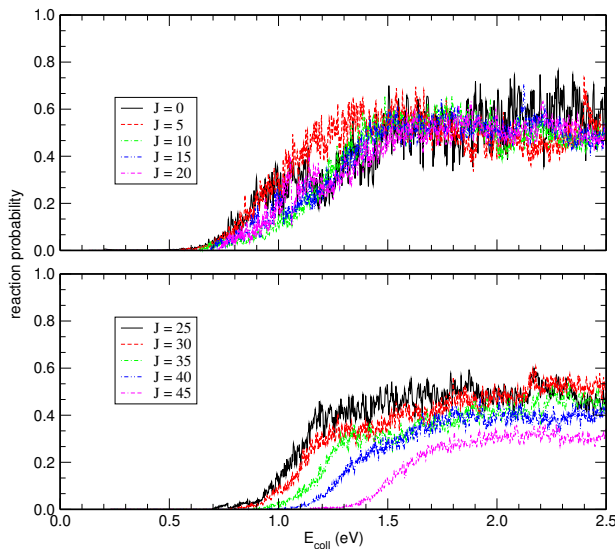


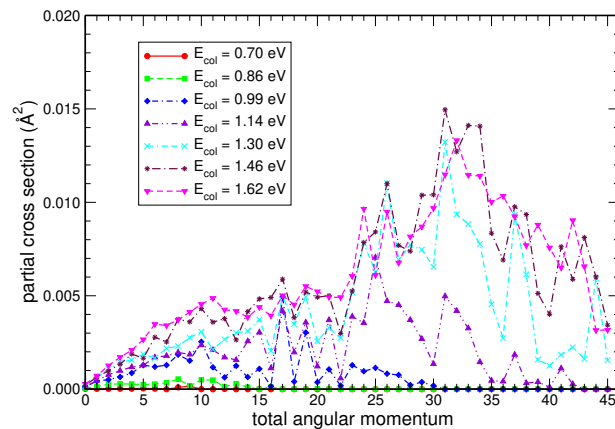
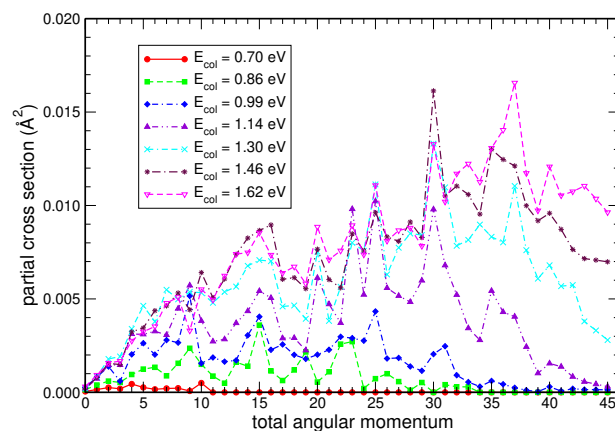
Fig. 1: Total reaction probabilities for H+O₂ ($v=0$, $j=1$) reaction performed on the CHIPR PES as a function of collision energy for $J=0, 5, 10, 15, 20, 25, 30, 35, 40$ and 45.

have depicted the profiles of partial cross sections for the reaction H+O₂ ($v=0$, $j=1$) at seven different collision energies, *viz.* $E_{col} \sim 0.70$ eV, 0.86 eV, 0.99 eV, 1.14 eV, 1.30 eV, 1.46 eV and 1.62 eV. It is quite clear from this plot that the partial cross sections generally increase with the collision energy. Moreover, the small values of the partial cross sections at very low energy ($E_{col} = 0.70$ eV) indicate the threshold value for opening the channel that yields O+OH (v', j') products. All profiles start with a small value at $J=0$ and then, gradually increase to a maximum, before finally diminishing at higher J s: a clear indication of the convergence of reaction probabilities with respect to total angular momentum. Note that the maxima of partial cross section profiles generally shifts towards the right hand side with increment of the collision energy. Note further from the profiles that with the increase of collision energy, the J s required for convergence of the partial cross sections generally increase. In Figure 5, the partial cross section profiles for the H+O₂ ($v = 0$, $j = 3$) reaction are displayed as a function of the total angular momentum for those seven different collision energies. On the other hand, the partial cross section profiles for the H+O₂ ($v = 0$, $j = 5$) reaction are depicted in Figure 6 for the same seven collision energies as in Figure 5. The general features for the $j = 5$ case are quite similar to those of the $j = 3$ case, except for the slightly higher magnitudes of the $j=5$ profiles with respect to the previous ones. It is also observed that the profiles for $j = 5$ converge somewhat faster than for both $j = 1$ and 3 cases, particularly at moderate collision energies (1.1 - 1.6 eV). Thus, the current calculation shows that in order to obtain converged reaction probabilities, FCC calculations are required upto at least upto $J=45$, a condition that may be judged at the same time as sufficient. It may be noted that due to the difficulty of performing fully close coupled (FCC) calculations by inclusion of all helicity quantum numbers for higher J s, we have restricted our study by considering total angular momenta upto 45. On the other hand, we had made an estimation

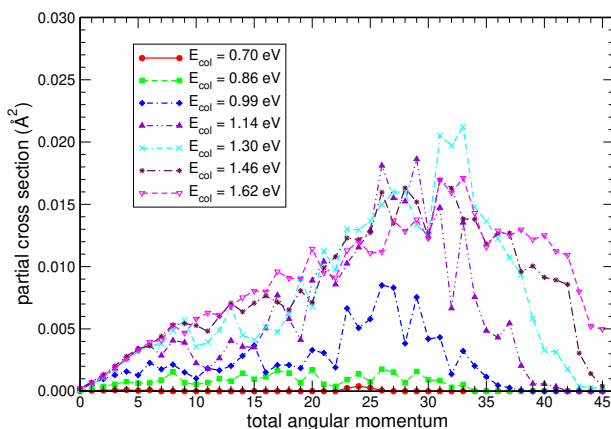
Fig. 2: Same as Fig. 1, but for $\text{H}+\text{O}_2$ ($v=0, j=3$) reaction.Fig. 3: Same as Fig. 1, but for $\text{H}+\text{O}_2$ ($v=0, j=5$) reaction.

of J_{\max} ($= 57$) elsewhere³⁸ by using the extrapolation scheme of Varandas,¹¹ where $J = 0$ quantum mechanical reaction probabilities were extrapolated with the help of QCT calculations. Since the correspondence principle suggests the quantum results gradually approach the corresponding classical ones with increasing energy, the estimation of J_{\max} by extrapolation scheme can be treated as an accurate one.

Figure 7 depicts the integral cross section for $\text{H}+\text{O}_2$ ($v=0, j=1$) reaction upto the collision energy of 2.5 eV. The general trend of the present profile is that it nearly increases monotonically with collision energy and then, reaches a maxima at around ~ 1.4 eV, before finally decreasing gently at higher collision energy regimes (1.4 – 2.5 eV). The profile for ICS shows reasonable agreement with our previously calculated profile³⁸ obtained by invoking the J -shifting approximation of Bowman³⁴ as well as Varandas' trajectory-based extrapolation scheme.¹¹ By closely looking into

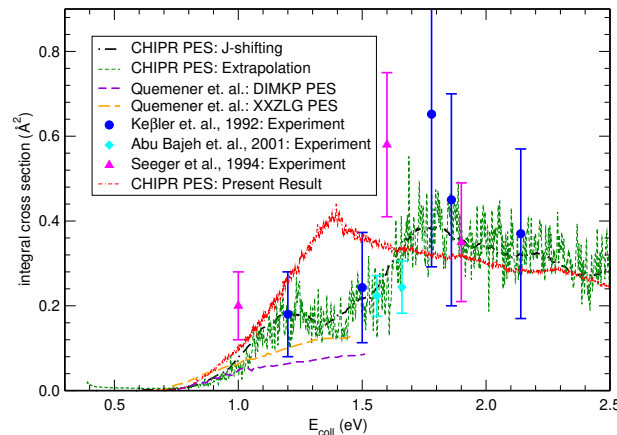
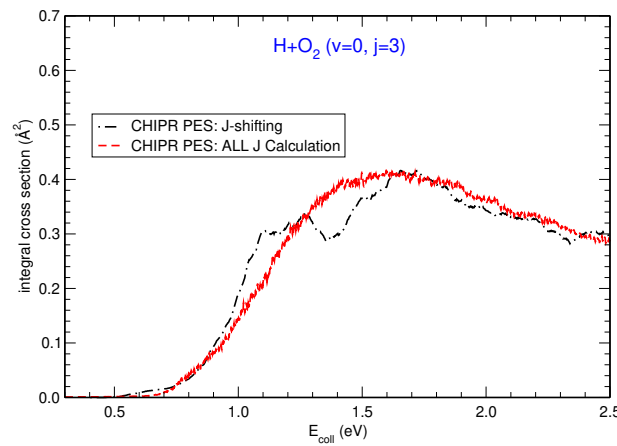
Fig. 4: Convergence of partial cross section with respect to total angular momentum for $\text{H}+\text{O}_2$ ($v=0, j=1$) reaction at six different collision energies.Fig. 5: Same as 4, but for $\text{H}+\text{O}_2$ ($v=0, j=3$) reaction.

those profiles, it is quite evident that the profile obtained by performing full J calculation matched well with both the J -shifting³⁸ and extrapolated curves in the lower energy regime (0.0 – 1.1 eV) not only in terms of magnitude but also in the trends of the profiles, while somewhat overestimating in the moderate energy regime (1.1 – 1.6 eV). Moreover, when the collision energy is increased further, the presently calculated ICS profile becomes a little bit lower than the previous ones. On the other hand, the time independent quantum dynamical calculations in low energy regimes performed by Quéméner *et al.* on the DIMKP PES as well as XXZLG PES²¹ and by Honvault *et al.*³¹ on the DMBE IV PES are lower estimating compared to our calculated profile as well as the previous calculations using both J -shifting and trajectory-based extrapolation.³⁸ It is noteworthy that the threshold value of the cross section is in good agreement with the previously calculated theoretical ones.^{21,31} Additionally, we have compared our results with the available experimental measurements of Keßler *et al.*,²² Abu Bajeh *et al.*,²³ and Seeger *et al.*²⁴ One can clearly notice that the present profile is having excellent agreement with that of Keßler *et al.*,²² in the entire energy regime and clearly falls within the error bars of the findings by Seeger *et al.*²⁴ in the higher energy regimes. Also, the trends of our ICS profiles

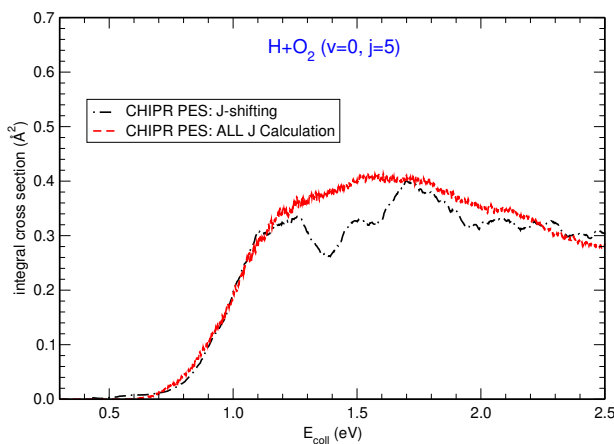
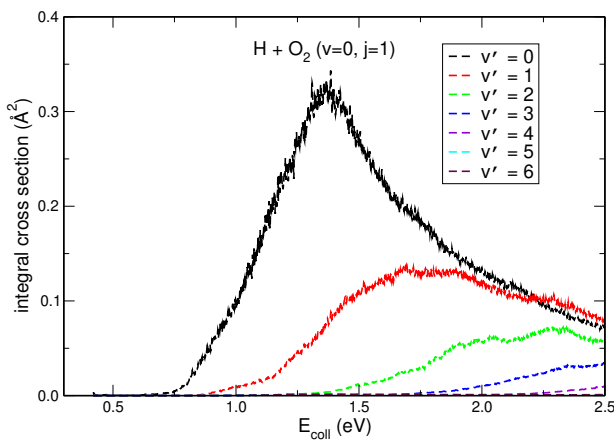
Fig. 6: Same as 4, but for $\text{H}+\text{O}_2$ ($v=0, j=5$) reaction.

are consistent with most available experimental results. On the other hand, the ICS profile for the $v=0, j=3$ rovibrational state is presented in Figure 8 in comparison with the previous profile obtained by J -shifting. Interestingly, the presently calculated profile is smoother than the J -shifting one. Although these two profiles show similar threshold values for the opening of the products channel, the visible humps in the previous profile (possibly arising from the $J=0$ reaction probability profile) are absent in the present case. Moreover, the magnitudes of the current profile at very low energies lie close to the J -shifting results, whereas, from moderate to high energies (1.2 – 2.5 eV), the present profile is generally higher than the J -shifting one. The ICS profile for $v=0, j=5$ case as shown in Figure 9 is quite similar to that of $j=3$ profile both in terms of trends and magnitudes. However, while comparing with the J -shifting result for the $v=0, j=5$ case, there is good agreement both in the very low and very high energy regimes (2.0 – 2.5 eV). Yet, the presently calculated profile generally depicts a greater magnitude from moderate to higher energy regimes (1.2 – 2.0 eV). Yet, the maxima in the ICS profile at around $E_{\text{col}} \sim 1.2$ eV for the J -shifting one is still missing when the dynamics is performed by inclusion of all non-zero total angular momentum situations. Moreover, the magnitudes of the ICS profiles increases minutely with the increment of initial rotational states, whereas the threshold value for the appearance of ICSs generally decreases with increasing j .

The close agreement of the current ICS profile with the corresponding experimental ones for the $\text{H}+\text{O}_2$ ($v=0, j=1$) reaction clearly indicates that calculations including all J s are necessary in order to obtain accurate integral cross sections, although both the J -shifting approximation³⁴ and Varandas' trajectory-based extrapolation technique¹¹ can be utilized to estimate approximate, yet quite reliable, values of such attributes. Indeed, the mismatch in the ICS profile obtained by J -shifting scheme with respect to the corresponding experimental measurements is overcome in the present calculation. Moreover, for the $v=0, j=1, 3$ and 5 cases, the noticeable differences between the J -shifting profile and calculated profile by FCC approach further suggests the necessity as well as stumps the credibility towards carrying out the dynamics for all nonzero J situations.

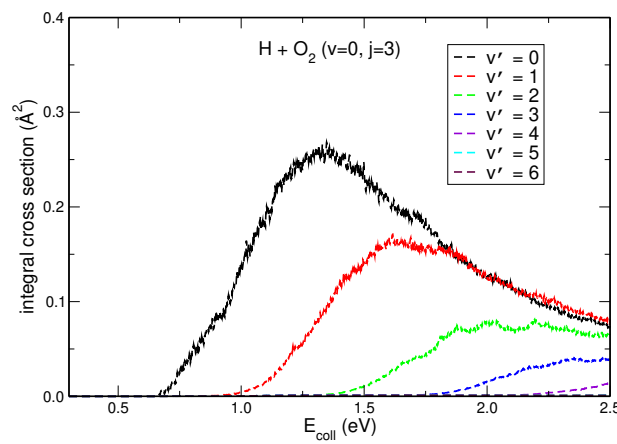
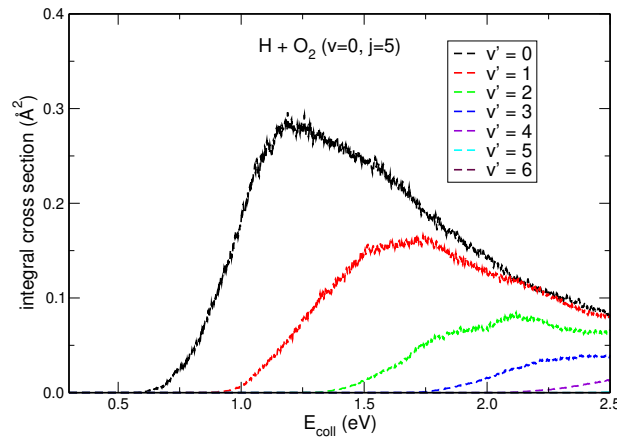
Fig. 7: Total integral cross section as a function of collision energy for $\text{H}+\text{O}_2$ ($v=0, j=1$) reaction in comparison with previous theoretical calculations and experimental measurements.Fig. 8: Same as Fig. 7, but for $\text{H}+\text{O}_2$ ($v=0, j=3$) reaction.

Vibrationally resolved integral cross sections for $\text{H}+\text{O}_2$ ($v=0, j=1$) reaction as a function of collision energy are presented in Figure 10. The ICS profiles for various v' 's start with different threshold values in ascending order and then gradually increase with collision energy before finally decreasing at higher collision energies. Moreover, the magnitude of the ICS decreases for higher v' states at almost all collision energies, except for the $v'=1$ state, which is showing slightly higher magnitude than that of $v'=0$ one after the collision energy of 2.2 eV. Although the calculations here reported upto $v'=10$ are included in our calculations, the vibrationally resolved ICSs for states above $v'=6$ are depicting very little magnitude indicating convergence of the profiles. The trends in the $j=3$ and $j=5$ profiles, shown respectively in Figures 11 and 12, are similar to the $j=1$ case. However, in this, the magnitude of the ICS for $v'=0$ and remaining v' states are higher and lower, respectively, when compared to the cases $j=3$ and 5. The initial state selected rate coefficients as function of inverse temperature are depicted in Figure 13 as an Arrhenius plot. Moreover, the corresponding results for the $\text{H}+\text{O}_2$ ($v=0, j=1, 3, 5$) reaction from previous theoretical calculations³⁸ employing the J -shifting approximation are put together for comparison. It is visible from panel-(a) that the presently calculated rate coeffi-

Fig. 9: Same as Fig. 7, but for $\text{H} + \text{O}_2$ ($v=0, j=5$) reaction.Fig. 10: Vibrationally resolved integral cross section as a function of collision energy for $\text{H} + \text{O}_2$ ($v=0, j=1$) $\rightarrow \text{O} + \text{OH}$ ($v'=0 - 6$, all j').

cient profile for $j=1$ case is showing slightly larger values at high temperature regimes and lower values for lower temperatures as compared to that of J -shifting. On the other hand, the mismatch in the rate coefficient profiles for $j=3$ and 5 in panel-(b) and (c), respectively, is much more prominent. In general, the comparison of these two cases ($j = 3$ and 5) with the J -shifting one shows that the former rate coefficient profiles exhibit a larger magnitude at almost all temperatures. Moreover, all these initial state selected rate coefficient profiles show that there is a slight increase of the rate constant with j at high temperatures, whereas at low temperatures the $j=3$ profile depicts a slightly lower magnitude. Note that the trends of the presently calculated initial state selected rate coefficients comply well with the results of Guo, Lendvay and coworkers¹⁹ as well as of Szabo et al.,⁶⁵ where it is found that the initial rotational excitation leads only to a small increase in the corresponding rate coefficient. The reader is referred to other papers^{66,67} for other commonly unexpected, yet numerically correct and justified, patterns.

Finally, Figure 14 shows the thermally averaged rate coefficient as obtained by Boltzmann averaging over the initial state ($j = 1, 3$ and 5) selected rate coefficients. In comparison, we have also plotted together with the thermal rate coefficient profiles of other

Fig. 11: Same as Fig. 10, but for $\text{H} + \text{O}_2$ ($v=0, j=3$) reaction.Fig. 12: Same as Fig. 12, but for $\text{H} + \text{O}_2$ ($v=0, j=5$) reaction.

theoretical results as well as available experimental data.^{35–37} Other theoretical calculations were performed on the CHIPR PES by time dependent³⁸ as well as time independent⁶⁸ quantum mechanical formalism and then, by utilizing J -shifting scheme.²¹ It is clear that the present profile differs significantly from the rate coefficient profiles calculated by the J -shifting scheme^{38,68} both in the moderate and high temperature regimes, but those profiles lie close in low to moderate temperatures ($T = 300 – 600$ K). Indeed, the slope of the Arrhenius plot in the present case is quite similar to those of the other theoretically calculated ones. Moreover, the present theoretically calculated rate coefficient for the title reaction is duly compared with the fitted experimental data obtained by Cohen and Westberg,³⁵ Baulch et al.,³⁶ Warnatz et al.³⁷ In the higher temperature regime, our calculated result matches quite well with that of Baulch et al., whereas the agreement with the results of Cohen and Westberg is good in moderate to high temperature regimes. Again, the data of Warnatz et al.³⁷ is generally higher estimating compared to our presently calculated profile. Finally, the disagreement with the previous theoretical calculations employing the J -shifting scheme and general good agreement with the experimental results underlines the importance of the FCC calculations for all non-zero J values: in spite of being computationally costly, they are necessary to accurately

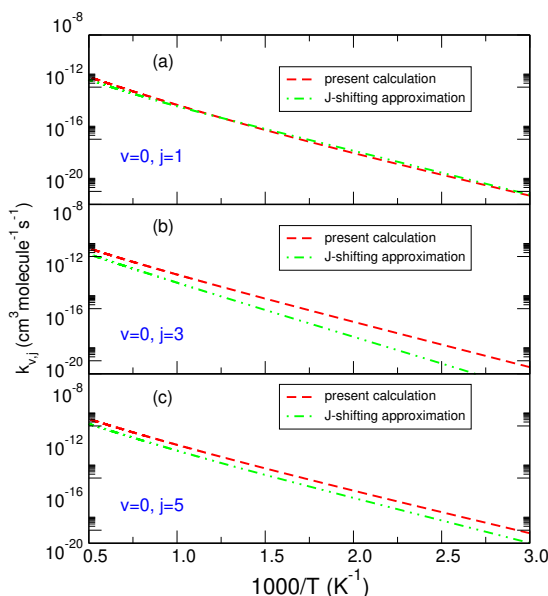


Fig. 13: Initial state selected rate coefficients as a function of inverse temperature for $\text{H} + \text{O}_2$ ($v=0$, $j=1, 3$ and 5) reaction in comparison with previous theoretical calculation.

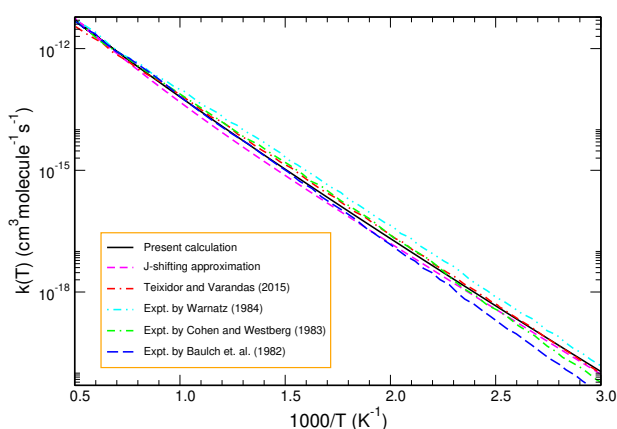


Fig. 14: Boltzmann averaged rate constant as a function of inverse temperature for $\text{H} + \text{O}_2$ reaction in comparison with previous theoretical calculations and experimental measurements.

estimate rate constants.

3 Summary

Time dependent wave-packet calculations for the reaction $\text{H} + \text{O}_2 \rightarrow \text{O} + \text{OH}$ have been carried out on the CHIPR PES by employing the FCC formalism, with a detailed investigation on the reactivity of this endoergic reaction performed for various initial rotational excitations of the O_2 molecule. A good correspondence has been found while comparing the important reaction attributes with those of previously reported TI^{21,68,69} and TD³⁸ calculations along with available experimental measurements.^{22–24,35–37} Despite showing some differences in the ICS profile for the $\text{H} + \text{O}_2$ ($v = 0, j = 1$) reaction carried out on CHIPR PES when compared with the results reported by Quéméner *et al.* in the DIMKP PES as well as XXZLG PES,²¹ significantly good agreement has been found with other theoretical calcula-

tions^{11,38} in the low energy regime and experimental measurements^{22,24} in the entire energy regime. On the other hand, a comparison of the presently calculated integral cross section profiles with those obtained by Bowman's *J*-shifting approximation as well as Varandas' trajectory-based extrapolation method¹¹ suggest two comments. The first to note their remarkable performance at low cost. The second, though, to note that the inclusion of total angular momenta beyond $J = 0$ is key to get good agreement with experimental data of cross sections for the title reaction, particularly at moderate to high collision energies. Similarly, thermal rate coefficient profiles calculated over the temperature range $300 – 2000\text{ K}$ clearly indicate the importance of including all non-zero J s. To sum up, significant improvement is achieved by performing higher- J calculations with the FCC approach, even if a daunting task in itself.

Acknowledgments

SG acknowledges IACS for research fellowship. SA acknowledges DST-SERB, India through project no. File No. EMR/2015/001314 for research funding and thanks IACS for access to the CRAY super-computing facility. A.J.C.V. thanks the support from China's Shandong Province "Double-Hundred Talent Plan" (2018), and Fundação para a Ciência e a Tecnologia, Portugal, via project UID/QUI/00313/2019.

References

- W. C. Gardiner, *Combustion Chemistry*, 1984, Springer, Berlin,
- H. Guo, *Int. Rev. Phys. Chem.*, 2012, **31**, 1–68.
- C. Xu, D. Xie, D. H. Zhang, S. Y. Lin and H. Guo, *J. Chem. Phys.*, 2005, **122**, 244305.
- A. J. C. Varandas, *J. Chem. Phys.*, 2013, **138**, 054120.
- C. F. Melius and R. J. Blint, *Chem. Phys. Lett.*, 1979, **64**, 183–189.
- M. R. Pastrana, L. A. M. Quintales, J. Brandao and A. J. C. Varandas, *J. Phys. Chem.*, 1990, **94**, 8073–8080.
- B. Kendrick and R. T. Pack, *J. Chem. Phys.*, 1995, **102**, 1994–2012.
- A. J. C. Varandas and A. I. Voronin, *J. Phys. Chem.*, 1995, **99**, 15846–15857.
- J. Troe and V. G. Ushakov, *J. Chem. Phys.*, 2001, **115**, 3621–3628.
- D. Xie, C. Xu, T. S. Ho, H. Rabitz, G. Lendvay, S. Y. Lin and H. Guo, *J. Chem. Phys.*, 2007, **126**, 074315.
- A. J. C. Varandas, *Molec. Phys.*, 1995, **85**, 1159–1164.
- A. J. C. Varandas, *Chem. Phys. Lett.*, 1995, **235**, 111–118.
- R. T. Pack, E. A. Butcher and G. A. Parker, *J. Chem. Phys.*, 1993, **99**, 9310–9313.
- R. T. Pack, E. A. Butcher and G. A. Parker, *J. Chem. Phys.*, 1995, **102**, 5998–6012.
- R. J. Duchovic and M. A. Parker, *J. Phys. Chem. A*, 2005, **109**, 5883–5896.
- S. Y. Lin, H. Guo, P. Honvaut and D. Xie, *J. Phys. Chem. B*, 2006, **110**, 23641–23643.

- 17 P. Bargueno, T. Gonzalez-Lezana, P. Larregaray, L. Bonnet and J. C. Rayez, *Phys. Chem. Chem. Phys.*, 2007, **9**, 1127–1137.
- 18 A. Viel, C. Leforestier and W. H. Miller, *J. Chem. Phys.*, 1998, **108**, 3489–3497.
- 19 S. Y. Lin, H. Guo, G. Lendvay and D. Xie, *Phys. Chem. Chem. Phys.*, 2009, **11**, 4715–4721.
- 20 S. Y. Lin, E. J. Rackham and H. Guo, *J. Phys. Chem. A*, 2006, **110**, 1534–1540.
- 21 G. Quemener, B. K. Kendrick and N. Balakrishnan, *J. Chem. Phys.*, 2010, **132**, 014302.
- 22 K. Keßler and K. Kleinermanns, *J. Chem. Phys.*, 1992, **97**, 374–377.
- 23 M. A. Bajeh, E. M. Goldfield, A. Hanf, C. Kappel, A. J. H. M. Meijer, H. R. Volpp and J. Wolfrum, *J. Phys. Chem. A*, 2001, **105**, 3359–3364.
- 24 S. Seeger, V. Sick, H. R. Volpp and J. Wolfrum, *Isr. J. Chem.*, 1994, **34**, 5–18.
- 25 S. Y. Lin, Z. Sun, H. Guo, D. H. Zhang, P. Honvault, D. Xie and S. Y. Lee, *J. Phys. Chem. A*, 2008, **112**, 602–611.
- 26 Z. Sun, D. H. Zhang, C. Xu, S. Zhou, D. Xie, G. Lendvay, S. Y. Lee, S. Y. Lin and H. Guo, *J. Am. Chem. Soc.*, 2008, **130**, 14962–14963.
- 27 A. J. H. M. Meijer and E. M. Goldfield, *J. Chem. Phys.*, 1998, **108**, 5404–5413.
- 28 A. J. H. M. Meijer and E. M. Goldfield, *J. Chem. Phys.*, 1999, **110**, 870–880.
- 29 E. M. Goldfield and A. J. H. M. Meijer, *J. Chem. Phys.*, 2000, **113**, 11055–11062.
- 30 M. Hankel, S. C. Smith and A. J. H. M. Meijer, *J. Chem. Phys.*, 2007, **127**, 064316.
- 31 P. Honvault, S. Y. Lin, d. Xie and H. Guo, *J. Phys. Chem. A*, 2007, **111**, 5349–5352.
- 32 A. J. C. Varandas, *J. Chem. Phys.*, 2013, **138**, 134117.
- 33 D. Skouteris, J. F. Castillo and D. Manolopoulos, *Comput. Phys. Commun.*, 2000, **133**, 128–135.
- 34 J. Bowman, *J. Phys. Chem.*, 1991, **95**, 4960–4968.
- 35 N. Cohen and K. R. Westberg, *J. Phys. Chem. Ref. Data*, 1983, **12**, 531–590.
- 36 D. L. Baulch, C. J. Cobos, R. A. Cox, P. Frank, G. Hayman, T. Just, J. A. Kerr, T. Murrells, M. J. Pilling, J. Troe, R. W. Walker and J. Warnatz, *J. Phys. Chem. Ref. Data*, 1994, **23**, 847–1033.
- 37 J. Warnatz, *Combustion Chemistry*, edited by W. C. Gardiner, Springer-Verlag, New York, 1984.
- 38 S. Ghosh, R. Sharma, S. Adhikari and A. J. C. Varandas, *Phys. Chem. Chem. Phys.*, 2018, **20**, 478–488.
- 39 S. Adhikari and A. J. C. Varandas, *Comput. Phys. Comm.*, 2013, **184**, 270–283.
- 40 T. Sahoo, S. Ghosh, S. Adhikari, R. Sharma and A. J. C. Varandas, *J. Phys. Chem. A*, 2014, **118**, 4837–4850.
- 41 S. Ghosh, T. Sahoo, S. Adhikari, R. Sharma and A. J. C. Varandas, *J. Phys. Chem. A*, 2015, **119**, 12392–12403.
- 42 D. Neuhauser, M. Baer, R. S. Judson and D. J. Kouri, *Chem. Phys. Lett.*, 1990, **169**, 372–379.
- 43 Y. Zhang, T.-X. Xie, K. L. Han and J. Z. H. Zhang, *J. Chem. Phys.*, 2003, **119**, 12921–12925.
- 44 T. S. Chu, T. X. Xie and K. L. Han, *J. Chem. Phys.*, 2004, **121**, 9352–9360.
- 45 R. F. Lu, T. S. Chu, Y. Zhang, K. L. Han, A. J. C. Varandas and J. Z. H. Zhang, *J. Chem. Phys.*, 2006, **125**, 133108.
- 46 S. G. Carrasco and O. Roncero, *J. Chem. Phys.*, 2006, **125**, 054102.
- 47 S. Y. Lin and H. Guo, *Phys. Rev. A*, 2006, **74**, 022703/1–8.
- 48 Z. Sun, X. Lin, S.-Y. Lee and D. H. Zhang, *J. Phys. Chem. A*, 2009, **113**, 4145–4154.
- 49 Z. Sun, H. Guo and D. H. Zhang, *J. Chem. Phys.*, 2010, **132**, 084112.
- 50 T. Sahoo, S. Ghosh, S. Adhikari, R. Sharma and A. J. C. Varandas, *J. Chem. Phys.*, 2015, **142**, 024304.
- 51 S. Ghosh, R. Sharma, S. Adhikari and A. J. C. Varandas, *Chem. Phys. Lett.*, 2017, **675**, 85–91.
- 52 G. D. Billing and N. Markovic, *J. Chem. Phys.*, 1994, **100**, 1085–1093.
- 53 J. D. Kress, R. T. Pack and G. A. Parker, *Chem. Phys. Lett.*, 1990, **170**, 306–310.
- 54 J. Crawford and G. A. Parker, *J. Chem. Phys.*, 2013, **138**, 054313.
- 55 H. Zhao, X. Hu, D. Xie and Z. Sun, *J. Chem. Phys.*, 2018, **149**, 174103/1–16.
- 56 S. Ghosh, S. Mukherjee, B. Mukherjee, S. Mandal, R. Sharma, P. Chaudhury and S. Adhikari, *J. Chem. Phys.*, 2017, **147**, 074105.
- 57 B. R. Johnson, *J. Chem. Phys.*, 1983, **79**, 1916–1925.
- 58 G. D. Billing and N. Markovic, *J. Chem. Phys.*, 1993, **99**, 2674–2681.
- 59 D. Neuhasuer and M. Baer, *J. Chem. Phys.*, 1989, **90**, 4351–4355.
- 60 N. Markovic and G. D. Billing, *Chem. Phys.*, 1995, **191**, 247–260.
- 61 D. Kosloff and R. Kosloff, *J. Comput. Phys.*, 1986, **52**, 35–53.
- 62 A. Viel, C. Leforestier and W. H. Miller, *J. Chem. Phys.*, 1998, **108**, 3489.
- 63 T. R. Rao, G. Guillon, S. Mahapatra and P. Honvault, *J. Chem. Phys.*, 2015, **142**, 174311/1–7.
- 64 Z. Sun, D. Yu, W. Xie, J. Hou, R. Dawes and H. Guo, *J. Chem. Phys.*, 2015, **142**, 174312/1–12.
- 65 P. Szabo and G. Lendvay, *J. Phys. Chem. A*, 2015, **119**, 7180–7189.
- 66 A. J. C. Varandas, T.-S. Chu, K.-L. Han and P. J. Caridade, *Chem. Phys. Lett.*, 2006, **421**, 415–420.
- 67 T.-S. Chu, K.-L. Han and A. J. C. Varandas, *J. Phys. Chem. A*, 2006, **110**, 1666–1671.
- 68 M. M. Teixidor and A. J. C. Varandas, *J. Chem. Phys.*, 2015, **142**, 014309.
- 69 M. M. Teixidor and A. J. C. Varandas, *Chem. Phys. Lett.*, 2015, **638**, 61–65.

